# X-ray spectral constraints on the magnetosphere structure of the unusual B0 V star $\tau$ Scorpii

David H. Cohen,[1][*] Richard H. D. Townsend,[2] Gregg A. Wade,[3]
*& others*, and the MiMeS Collaboration
[1]*Swarthmore College, Department of Physics and Astronomy, Swarthmore, Pennsylvania 19081, USA*
[2]*University of Wisconsin, Madison, Department of Astronomy, Madison, Wisconsin 53711, USA*
[3]*Royal Military College of Canada, Department of Physics, Kingston, Ontario, Canada*

19 July 2011

**ABSTRACT**

We evaluate the conditions under which the hard and strong X-ray emission from $\tau$ Sco could arise in the confined portions of the star's magnetosphere. The Mg XI complex near 9.2 Å measured with the *Chandra* grating spectrometer provides the strongest constraint of $2.4 < r/R_* < 2.9$ for the emission measure weighted mean location of the multi-million K plasma emitting the observed thermal X-rays. We present new field extrapolations based on spectropolarimetric maps of the surface field, which assume larger source surfaces than have been used previously. We find that these magnetospheric reconstructions can accommodate X-ray emitting plasma within their closed-field regions at distances of several stellar radii when source surface radii of $\sim 5$ are used in the reconstruction. Such values are consistent with the new, lower mass-loss rate determination of the wind of $\tau$ Sco.

**Key words:** stars: early-type – stars: magnetic field – stars: winds, outflows – stars: individual: $\tau$ Sco – X-rays: stars

## 1 INTRODUCTION

$\tau$ Sco is a strong X-ray emitter (Cohen et al. 1997a,b; Mewe et al. 2003; Cohen et al. 2003), with a complex magnetic field (Donati et al. 2006). It is often assumed that the X-ray emitting plasma is associated with the magnetosphere of the star, but recent multiphase X-ray observations of $\tau$ Sco (Ignace et al. 2010) failed to show the rotational modulation expected if the hot plasma is confined to the closed-field regions in the magnetosphere topology computed by Donati et al. (2006). This magnetosphere topology is computed using a potential field extrapolation constrained by Magnetic Doppler Imaging (MDI) measurements of the surface field strength distribution, which provide a lower boundary condition, and assuming a source surface located at $r = R_{\rm source} = 2R_*$ as the outer boundary condition (Jardine et al. 1999; Donati et al. 2006). The physical implication of the source surface constraint is that all field lines are purely radial at that location, and thus all the closed magnetic loops are inside the source surface. In this letter, we compute alternate field topologies for the magnetosphere using different source surface locations in an attempt to determine the requirements

for a magnetospheric topology that is consistent with X-ray observations.

While the lack of rotational modulation of the observed X-rays shows that they are not produced within the closed magnetic loops shown in figure 11 of Donati et al. (2006), in principle, more specific information about the location of the hot plasma is provided by the forbidden-to-intercombination line ratios of helium-like species observed in high-resolution X-ray spectra (Porquet et al. 2001). These line ratios are a function of the local ultraviolet (UV) mean intensity at the location of the X-ray emitting plasma, and so depend on the distance of the plasma from the photosphere, given an assumed UV surface flux. In this letter we also reanalyze the helium-like line ratios measured with the *Chandra* grating spectrometer to determine where the X-rays observed from $\tau$ Sco are produced. If the X-rays are produced in the closed-field regions of the magnetosphere, via Magnetically Channeled Wind Shocks (MCWS) (Babel & Montmerle 1997; ud-Doula & Owocki 2002; Gagné et al. 2005; Townsend et al. 2007), then these X-ray line ratios can help determine which field models could describe the magnetosphere of $\tau$ Sco.

In §2 we present the potential field modeling of the magnetosphere. In §3 we present the analysis of the helium-like X-ray lines. And in §4 we discuss what the modeling,

[*] E-mail: cohen@astro.swarthmore.edu

spectral analysis, and other observational constraints imply about the actual magnetosphere of $\tau$ Sco and about the mechanism that generates its strong X-ray emission. We summarize our conclusions in §5

## 2 THE MAGNETIC FIELD

*This section is unchanged from the previous version. Except for one sentence cut from the first paragraph.*

$\tau$ Sco is one of only a handful of massive stars earlier than spectral type B2 on which a magnetic field has been detected. Unlike most of the other O and very early B stars with magnetic fields, $\tau$ Sco does not have a predominantly dipole field, but rather has a highly spatially structured field. This determination was made from a rich set of spectropolarimetric observations, well sampling the 41 day rotation period of the star (Donati et al. 2006). Maps of the surface field strength, broken down into radial, azimuthal, and meridional components, are shown in figure 8 of Donati et al. (2006) and clearly demonstrate that the field is more spatially complex than a simple dipole.

The magnetic field structure above the photosphere can be modeled using the surface field map as a lower boundary condition, and by describing the field via a sum of spherical harmonics (Donati et al. 2006; Jardine et al. 1999). The field extrapolation requires an outer boundary condition, which is provided by a source surface, at which location it is assumed that all field lines are purely radial. This constrains all closed-field regions to be below the source surface. In Donati et al. (2006), the source surface was assumed to be at $R_{\mathrm{source}} = 2\,R_*$, based on the expected wind confinement, assuming a mass-loss rate of $2 \times 10^{-8}\,\mathrm{M_\odot\,yr^{-1}}$. But as those authors point out, if the mass-loss rate is lower, the confinement will be correspondingly higher and the field will remain closed to larger radii (the Alfvén radius will be larger). Indeed, a recent detailed analysis of the UV spectrum of $\tau$ Sco indicates that the wind mass-loss rate is likely more than an order of magnitude lower (Petit et al. 2011; Oskinova et al. 2011), and thus the closed field region may extend to many stellar radii.

We have recomputed the field structure, using the same potential field extrapolation technique, and using the surface field map presented by Donati et al. (2006). We initially employed the same source surface radius of $R_{\mathrm{source}} = 2\,R_*$. Our results, shown in Fig. 1, are very similar to those presented by Donati et al. (2006). The reconstruction shows closed magnetic loops only within the first stellar radius above the photosphere, and organized into a band nearly perpendicular to the star's equator, and a large patch of closed loops at mid-latitudes. The star is seen close to equator on, and thus rotation will significantly modulate the fraction of the closed magnetic loops visible to an observer.

We next present magnetic field reconstructions in Fig. 2 assuming larger source surface radii, of $R_{\mathrm{source}} = 4\,R_*$ and $6\,R_*$. Indeed, these larger source surface radii do allow for larger closed field regions, with loops extending several stellar radii above the surface of $\tau$ Sco. In the $R_{\mathrm{source}} = 4\,R_*$ case and especially in the $R_{\mathrm{source}} = 6\,R_*$ case, most of the large closed loop regions are near the poles, and will not
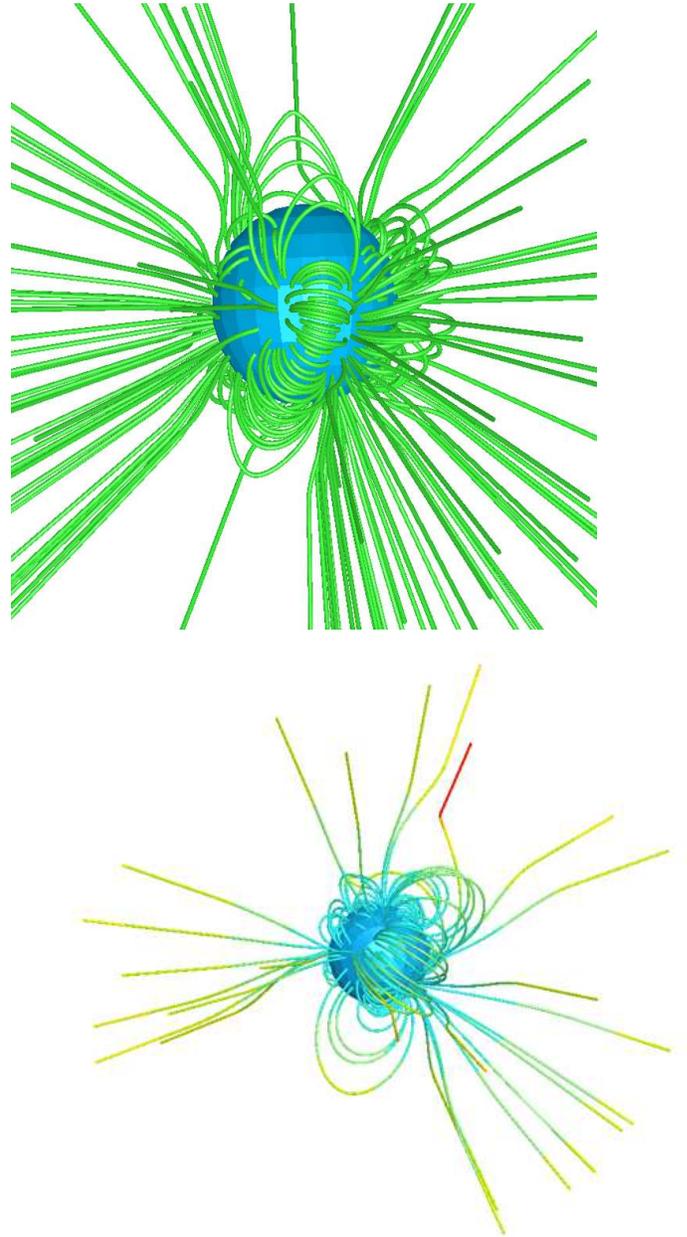


**Figure 1.** Our reconstruction of the magnetic field structure above the photosphere, based on the surface field maps shown in figure 8 of (Donati et al. 2006). **I suppose we will replace this figure and the snapshots in the next figure with some version of Rich's new figure (the initial version of which is redundantly shown in the bottom panel), showing the local $\eta$ in each field line; and standardizing the viewing geometry, etc.**

be rotationally modulated. Actually computing the distribution of X-ray emitting plasma within each loop is currently not tractable. But there are constraints available from X-ray spectroscopy.
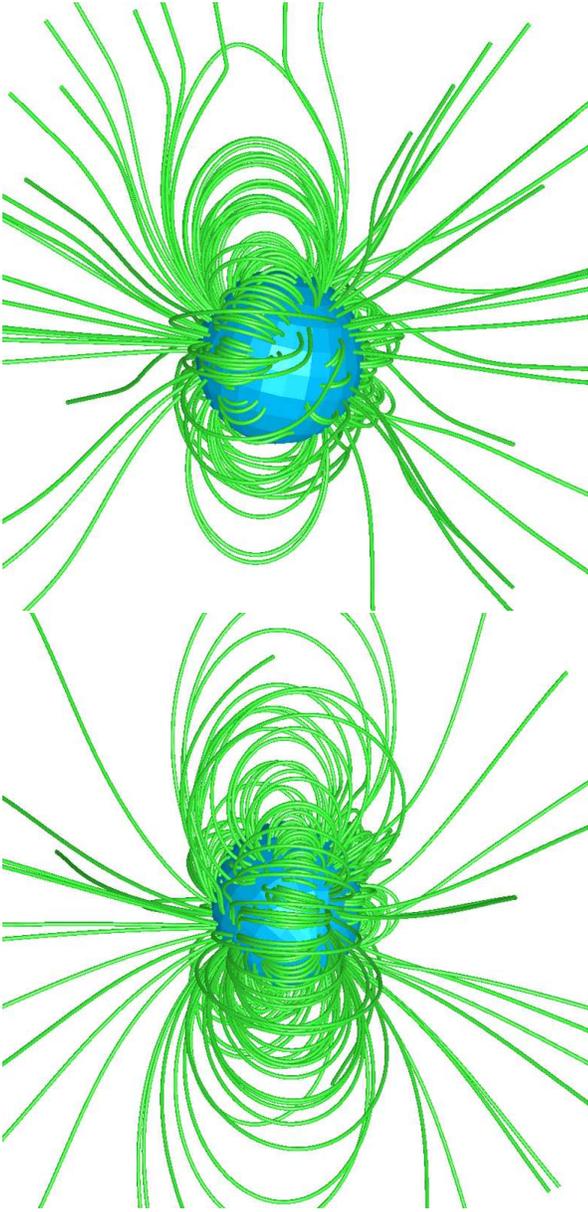
**Figure 2.** Field reconstructions analogous to the one shown in Fig. 1, but for larger values of the source surface radius: $R_{\rm source} = 4\ R_*$ (top) and $R_{\rm source} = 6\ R_*$ (bottom). Note that the closed field regions extend to larger radii as the source surface location moves away from the photosphere.

## 3   HELIUM-LIKE X-RAY LINE RATIO DIAGNOSTICS

The forbidden $1s2s\ ^3S_1 - ^1S_0$ line of He-like ions (e.g. Ne IX, Mg XI, Si XIII, S XV, observed between 1 and 2 keV) can be weakened with respect to the nearby intercombination line ($1s2p\ ^3P_{1,2} - ^1S_0$) if the local UV radiation field is strong enough to drive the transition from the metastable upper level of the forbidden line to the upper level of the intercombination line. The extent to which the UV photoexcitation alters the forbidden-to-intercombination ($f/i$) line ratio depends on the distance of the X-ray emitting plasma from the photosphere and on the emergent photo-

spheric UV flux at the wavelengths of the particular transitions, which are different for each element. Thus, an observed $f/i$ line ratio (referred to as $\mathcal{R} \equiv f/i$) is an emission measure weighted average over a distribution of hot plasma above the photosphere. The contribution from each radius is given by $\mathcal{R} = \mathcal{R}_o/(1 + 2PW)$ (see Leutenegger et al. (2006), equation 3). Here, $\mathcal{R}_o$ is the "zero-flux limit" of the line ratio[1], and $W$ is the geometrical dilution factor, $W = 0.5(1 - \sqrt{1 - (R_*/r)^2})$. $P$ depends on atomic physics – including the *f-value* of the UV transition – and the surface Eddington flux, $H_\nu$, at the frequency of the $^3P_{1,2}$ transitions. Thus, by adopting atomic physics parameters – here taken from Blumenthal et al. (1972); Dere et al. (2007); Porquet et al. (2001) as in Leutenegger et al. (2006) – and a model atmosphere, we can find the radius that best reproduces the observed $f/i$ line ratio.

In this letter, we use *Chandra* High Energy Transmission Grating Spectrometer (HETGS) data from two observations (ObsIDs 638 and 2305, taken 17 - 18 September 2000) with a total effective exposure time of 72,130 s. We fit the Medium Energy Grating (MEG) and High Energy Grating (HEG) data simultaneously in XSPEC v12.6. We use the C statistic (Cash 1979) to place confidence limits on the model parameters of interest, using the formalism described in Press et al. (2007).

We fit the He-like line complexes using three Gaussian line profiles, with their width and centroid shift parameters tied together (but free to vary in the fit). The other parameters of the model are the line normalizations, expressed as $\mathcal{R} = f/i$, $\mathcal{G} = (f + i)/r$, and the total normalization, where $f$, $i$, and $r$ denote the fluxes of the forbidden, intercombination, and resonance lines, respectively. The model also includes a power-law to fit the underlying continuum. The level of the continuum model component is determined by fitting line-free regions of the spectrum near each line complex prior to fitting the line complexes themselves.

The Mg XI and Si XIII complexes provide the only useful constraints on the plasma location in $\tau$ Sco, and we show the results of fitting these two complexes in Figs. 3 and 4. To model the $f/i$ ratio we use a TLUSTY model atmosphere (Lanz & Hubeny 2003) as the source of the relevant UV fluxes. The UV wavelengths of the photoexcitation transitions are 997 and 1034 Å for Mg XI and 814 and 865 Å for Si XIII. Donati et al. (2006) derive $T_{\rm eff} = 31{,}000$ K and $log\ g = 4.25$ for $\tau$ Sco. This effective temperature lies between the 30,000 K and 32,500 K models on the TLUSTY grid, and so we use both model atmospheres to bracket our results. At the wavelengths that excite the Mg XI transitions, the model atmospheres have very similar fluxes, but the Si XIII transitions are below the Lyman edge, and there the fluxes predicted by the two model atmospheres differ by more than a factor of three. So, for Si XIII we make two plasma location determinations, one for each model atmosphere.

The Mg XI $f/i$ ratio is significantly altered from the zero-flux limit of $\mathcal{R} = \mathcal{R}_o = 2.7$. We find $\mathcal{R} = f/i = 0.38 \pm .07$ (68 percent confidence limit). Using eqn. 3 of

---

[1] In other words, it is what $\mathcal{R} = f/i$ would be in the absence of any UV photoexcitation. this is equivalent to the "low-density limit" when this line ratio is employed as a density diagnostic.
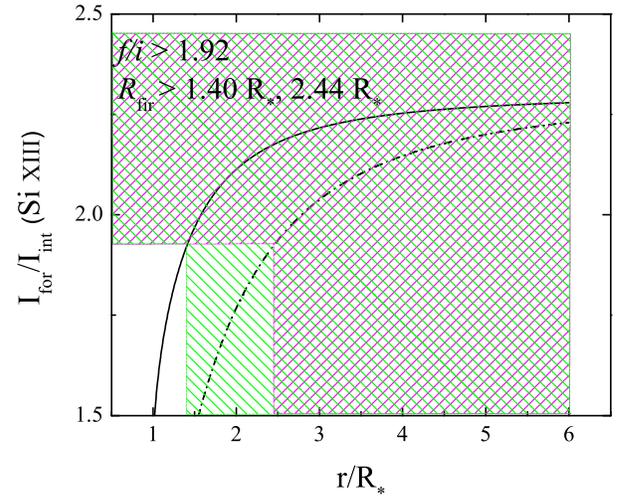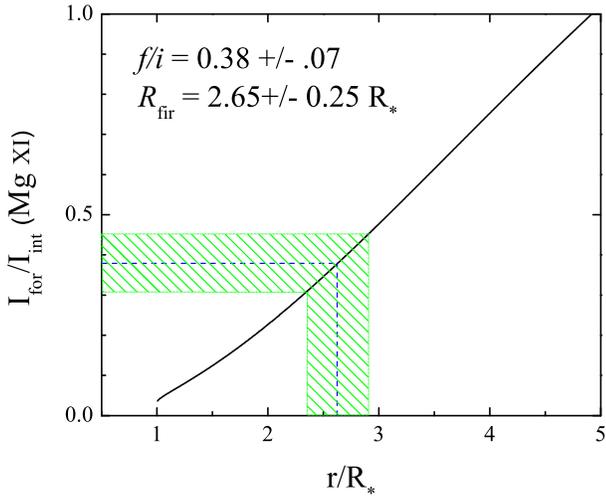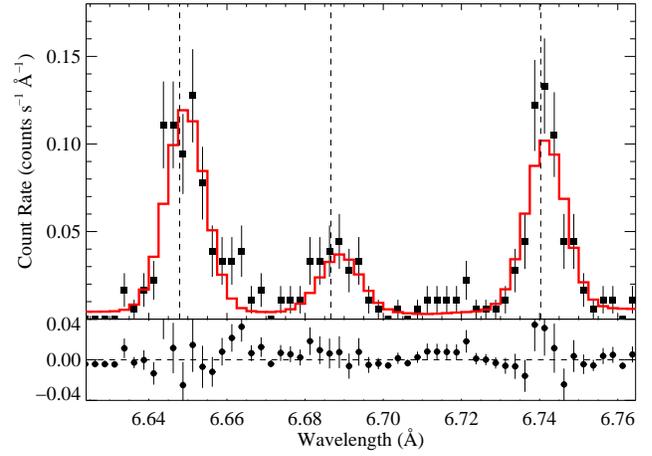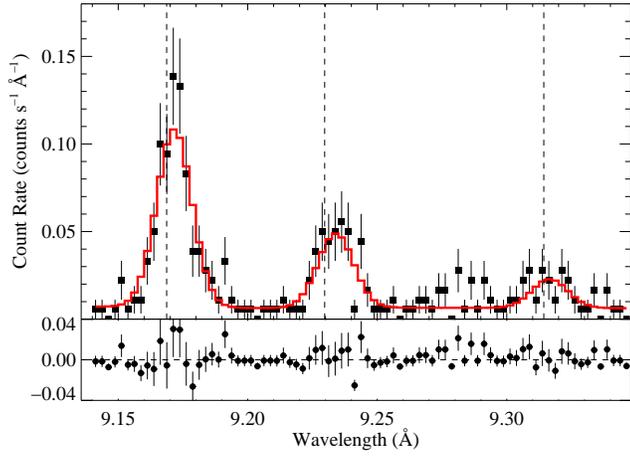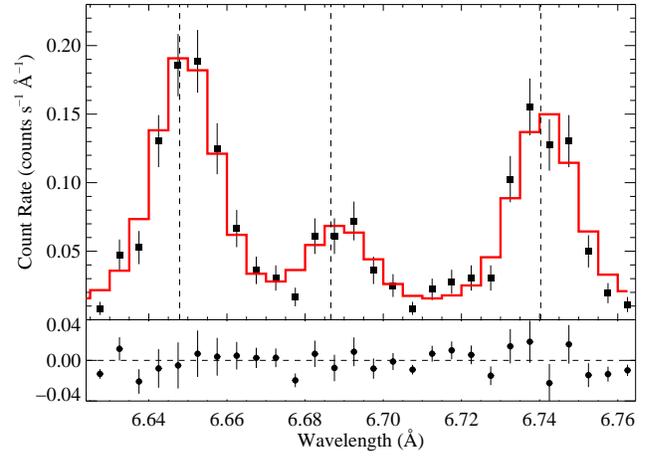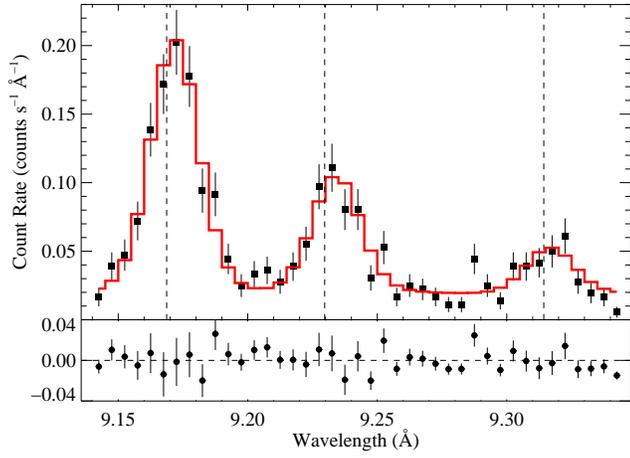
**Figure 3.** Mg XI resonance, intercombination, and forbidden lines (from short to long wavelength) measured in the MEG (top) and HEG (middle), with data shown as points with Poisson error bars. The best-fit model is shown as a red histogram. The bottom panel shows the constraints on the source location. The solid curve is the relationship between the $f/i$ ratio and the location of the X-ray emitting plasma. The best-fit $f/i$ ratio is indicated by the blue dashed horizontal line, and the vertical line shows the corresponding best-fit plasma location. The 68 percent confidence limits are indicated by the green cross-hatched region.

**Figure 4.** The Si XIII resonance, intercombination, and forbidden line complex, and constraints. The constraints are based on a lower limit to the measured line ratio of $f/i = 1.92$, which corresponds to a lower limit on the formation radius of $r > 1.40\ R_*$ given the cooler model atmosphere (green) and $r > 2.44\ R_*$ given the hotter model atmosphere (pink).

Leutenegger et al. (2006), we compute the run of $f/i$ vs. radius, which we show, along with the measured $f/i$ constraints, in the lower panel of Fig. 3. The corresponding emission radius is $r = R_{\rm fir} = 2.65 \pm .25\ R_*$. For Si XIII, the best-fit value is $\mathcal{R} = f/i = 2.17^{+.28}_{-.25}$, which is consistent with the low-flux limit of $\mathcal{R} = \mathcal{R}_o = 2.3$. This measurement thus provides a lower limit on the emission radius. To compute this limit, we use the 68 percent lower confidence limit on the measured line ratio of $\mathcal{R} = f/i = 1.92$. The constraints are shown in the lower panel of Fig. 4 and correspond to $r = R_{\rm fir} > 1.40\ R_*$ for the $T_{\rm eff} = 30,000$ K atmosphere and $r = R_{\rm fir} > 2.44\ R_*$ for the $T_{\rm eff} = 32,500$ K atmosphere.

The lower limits from the Si XIII complex are consistent with the constraints from the Mg XI complex, although it is possible for the line complexes to be formed in spatially distinct regions. It is probable, however, that they are largely co-spatial, as their temperature dependencies are similar (peak emissivity of the Mg XI lines is at $\log T = 6.8$ while for the Si XIII lines it is at $\log T = 7.0$). Thus, the simplest interpretation of the X-ray spectral constraints is that the X-ray emitting plasma is, on average, at $r = 2.65 \pm .25\ R_*$, or $1.65 \pm .25\ R_*$ above the photosphere of $\tau$ Sco.

## 4  DISCUSSION

*This section is unchanged from the previous version.*

The location of the hot, X-ray emitting plasma on $\tau$ Sco is consistent with an origin in the closed-field regions of the star's magnetosphere, given the constraints of the measured surface magnetic field in the context of a potential field extrapolation that assumes a source surface radius of at least $R_{\rm source} = 4\ R_*$. And this larger source surface radius is consistent with recent determinations of the star's wind mass-loss rate. The closed-field regions are where X-ray emission is expected to arise in the context of the MCWS mechanism, in which wind flows up the footpoints of closed magnetic loops, is accelerated to high velocities, and then collides and shocks at the top of the loop. For this mechanism to produce hard X-rays, high flow velocities are required. The $T \approx 10^7$ K temperatures inferred from the X-ray spectrum require shock velocities of roughly 1000 km s$^{-1}$, which is an appreciable fraction of the wind terminal velocity for $\tau$ Sco, and thus large loops (of order a stellar radius or more in size) are required simply to explain the observed X-ray temperatures.

The larger loops seen in the field extrapolations shown in Fig. 2 are certainly big enough to accommodate such high-speed flows and shocks, as well as providing consistency with the $f/i$ ratios and the lack of rotational modulation of the X-rays. Detailed 3-D MHD simulations will ultimately be required to see if enough X-ray emission can be produced with the observed temperature distribution and over a range of locations consistent with the $f/i$ ratios and lack of X-ray time variability. If the MCWS scenario applies to the X-rays from $\tau$ Sco, it is important to note that unlike the rapidly rotating Bp star, $\sigma$ Ori E, there will not be any significant centrifugal support for the magnetospheric plasma in $\tau$ Sco. Rather, the shock heated and cooling plasma will likely be falling back down the field lines, onto the star, much like what is seen in simulations of the slowly rotating magnetic O star, $\theta^1$ Ori C.

**Other Issues:**

Such infall may also play a role in explaining the unusual read-shifted absorption signatures seen in high ion stages in the UV spectra of $\tau$ Sco.

**Where/how to include Rich's new field modeling? Sec. 2? Certainly the discussion will also have to be updated (and some of the items in this list included as well).**

Overall X-ray emission measure/luminosity – to what extent does this provide constraints on (or problems understanding) the mass-loss rate (i.e. is the X-ray luminosity too high to be understood in terms of MCWS if the mass-loss rate is low)?

Other lines of evidence? ...X-ray variability (stochastic, with 10 to 20 percent variability; more variable than normal O stars); differential emission measure modeling and implications.

The X-ray lines are quite narrow – this is consistent with wind confinement, but what about other late O and early B stars that are not seen to be magnetic but which also show quite narrow X-ray lines? Maybe the X-rays do not, after all, come from the closed-field regions and via MCWS. (On the other hand, the X-rays in those other stars – $\sigma$ Ori A, $\beta$ Cru – are softer than those seen in $\tau$ Sco. However, these stars, while not having *detected* magnetic fields could still have fields, and in fact, could have confinement parameters above unity, but just haven't had their fields detected yet.)

Comparisons/improvements with respect to previous $f/i$ analysis (in Cohen et al. (2003)).

## 5  CONCLUSIONS

**REFERENCES**

Babel J., Montmerle T., 1997, ApJ, 485, L29
Blumenthal G. R., Drake G. W. F., Tucker W. H., 1972, ApJ, 172, 205
Cash W., 1979, ApJ, 228, 939
Cohen D. H., Cassinelli J. P., MacFarlane J. J., 1997, ApJ, 487, 867
Cohen D. H., Cassinelli J. P., Waldron W. L., 1997, ApJ, 488, 397
Cohen D. H., de Messières G. E., MacFarlane J. J., Miller N. A., Cassinelli J. P., Owocki S. P., Liedahl D. A., 2003, ApJ, 586, 495
Dere K. P., Landi E., Young P. R., Del Zanna G., Landini M., Mason H. E., 2007, A&A, 498, 915

Donati J.-F., et al., 2006, MNRAS, 370, 629

Gagné M., Oksala M., Cohen D. H., Tonnesen S. K., ud-Doula A., Owocki S. P., Townsend R. H. D., MacFarlane J. J., 2005, ApJ, 628, 986

Ignace R., Oskinova L. M., Jardine M., Cassinelli J. P., Cohen D. H., Donati J.-F., Townsend R. H. D., ud-Doula A., 2010, ApJ, 721, 1412

Jardine M., Barnes J., Donati J.-F., Collier Cameron A., 1999, MNRAS, 305, L35

Lanz T., Hubeny I., 2003, ApJS, 146, 417

Leutenegger M. A., Paerels F. B. S., Kahn S. M., Cohen D. H., 2006, ApJ, 650, 1096

Mewe R., Raassen A. J. J., Cassinelli J. P., van der Hucht K. A., Güdel M., 2003, A&A, 398, 203

Oskinova L. M., Todt H., Ignace R., Brown J. C., Cassinelli J. P., Hamann W.-R., 2011, MNRAS, in press

Petit V., Massa D. L., Marcolino W. L. F., Wade G. A., Ignace R., 2011, MNRAS, 412, L45

Porquet D., Mewe R., Dubau J., Raassen A. J. J., Kaastra J. S., 2001, A&A, 376, 1113

Press W. H., Flannery B. P., Teukolsky S. A., Vetterling W. T., 2007, Numerical Recipes, $3^{rd}$ edition. Cambridge University Press, Cambridge

Townsend R. H. D., Owocki S. P., ud-Doula A., MNRAS, 382, 139

ud-Doula A., Owocki S.P., 2002, ApJ, 576, 413